Supplementary Information for

Measurements of Aptamer-Protein Binding Kinetics Using Graphene Field-Effect Transistors

Xuejun Wang[a,b], Zhuang Hao[a], Timothy R. Olsen[a], Wenjun Zhang[c], Qiao Lin[a]*

[a]Department of Mechanical Engineering, Columbia University, New York, NY 10027, USA
[b]State Key Laboratory of Molecular Engineering of Polymers, Department of Macromolecular Science, Fudan University, Shanghai, 200438, China
[c]Department of Mechanical Engineering, University of Saskatchewan, Saskatoon, S7N 5A9, Canada

Device fabrication: The device was fabricated via a thermally assisted bilayer lift-off process (Fig. S1). Two layers of resist (sacrificial layer LOR and photoresist S1811) were sequentially spin-coated on the wafer. After exposure and development, 5/45 nm Cr/Au were deposited using thermal evaporation. The sample was heat-treated on a hot plate at 170 °C for 2 min to allow photoresist reflow. Due to the higher reflow temperature of LOR (MicroChem LOR™ series reflow temperature > 250 °C, DOW MicroPosit S1800 series reflow temperature < 200 °C), the bottom photoresist undercut remains undeformed while the top layer deformed. The introduced gap allowed a stripper solution to access the photoresist, and tremendously improved the efficiency of lift-off process. The sample was exposed to oxygen plasma to remove remaining residue. Graphene synthesized via chemical vapor deposition (CVD) was then transferred onto the target substrate using a poly(methyl methacrylate) carrier layer (PMMA) to connect the drain and source electrodes by following a previously reported protocol.[1] Then the carrier layer PMMA carrier was removed by acetone. The graphene was eventually patterned to define the sensing region.

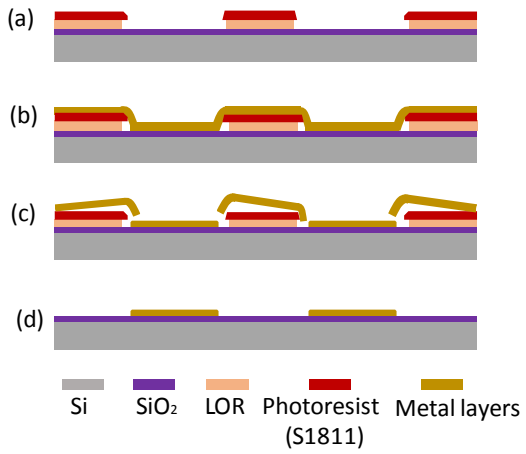

Fig. S1 Thermal-assisted lift-off method. (a) Spin-coating of sacrificial layer LOR and photoresist S1811. (b) Metal deposition. (c) Thermal reflow of photoresist. (d) Photoresist lift off.

Biochemical functionalization: To functionalize the surface for binding characterization studies (Fig. S2), the GFET was first immersed for 2 hours at room temperature in a dimethylformamide (DMF) solution of 5 mM 1-pyrenebutanoic acid succinimidyl ester (PASE), which serves as a linker. The linker was terminated to the graphene via π-π interaction of pyrene group with graphene. After rinsing thoroughly with ethanol, phosphate buffered saline (PBS) buffer, and a 1 μM solution of IgE-specific D17.4 aptamer in PBS was added to the channel of the GFET for 12 hours at

room temperature. Following this incubation, 100 mM ethanolamine was added to the graphene channel for 1 hour to deactivate and block the excess reactive groups remaining on the graphene surface.

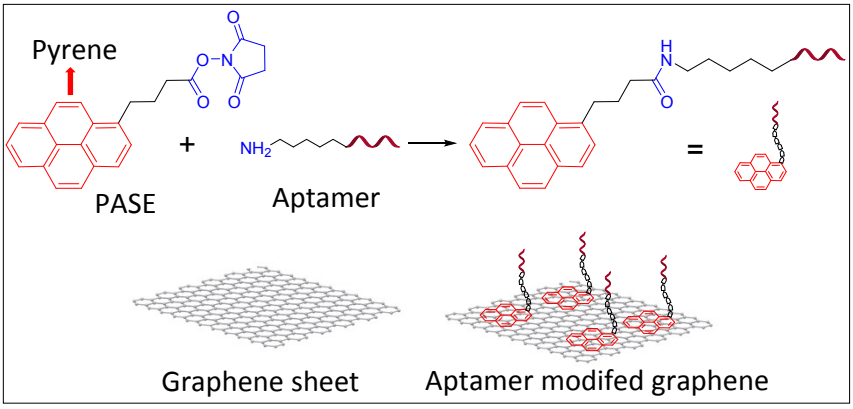

Fig. S2 Biochemical immobilization of graphene. Aptamer was functionalized on graphene via the PASE linker that was terminated to the graphene surface via π-π interaction between the pyrene group with graphene. (with ethanolamine blocking).

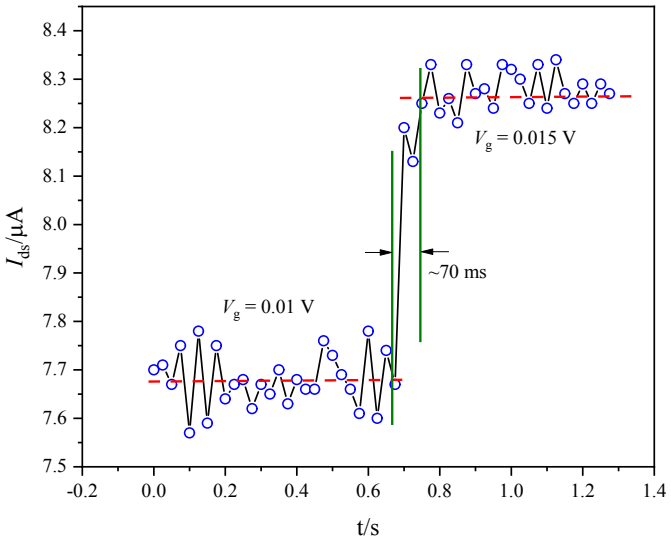

Fig. S3. Response time of the GFET nanosensor to the increased gate voltage.

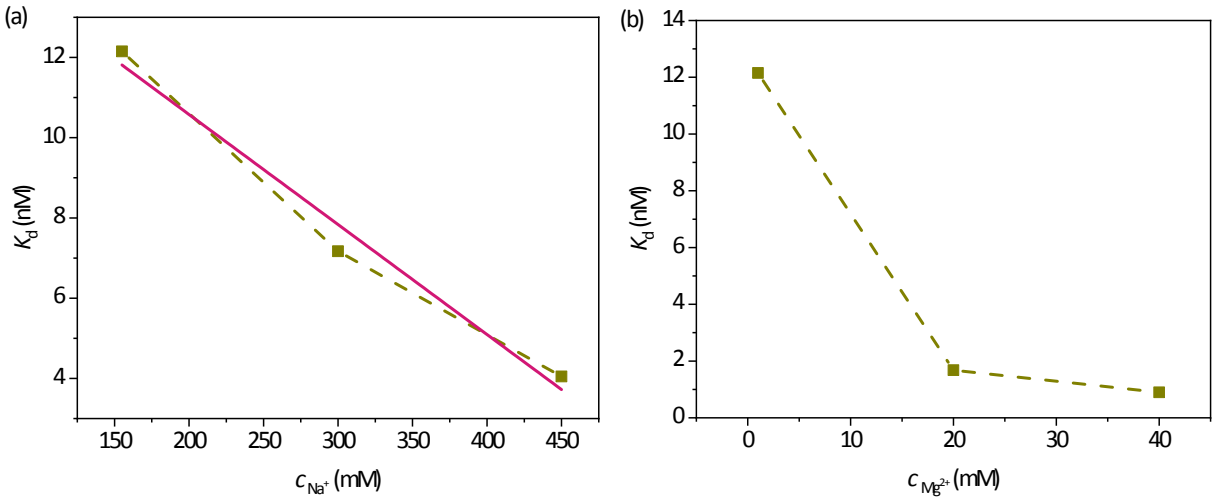

Fig. S4 The equilibrium dissociation constant K_d of the aptamer-IgE binding system as a function of different (a) Mg^{2+} and (b) Na^+ concentrations.

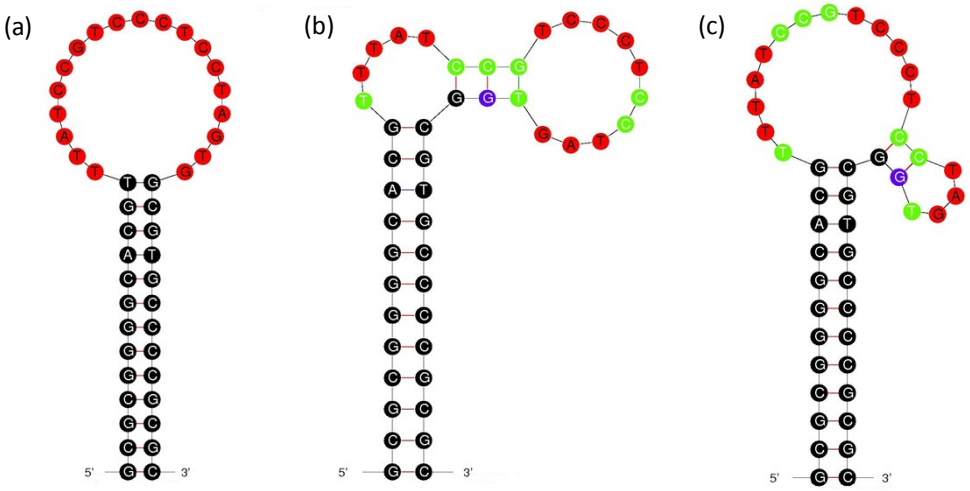

Fig. S5 Predicted secondary structures of IgE aptamer at Mg^{2+} concentrations of (a) 1 mM, (b) 20 mM and (c) 40 mM, with Na^+ concentration of 161 mM and temperature at 20℃.

Temperature control set-up: Closed-loop temperature control of the chamber was achieved by the integrated temperature sensor and Peltier module with a proportional-integral-derivative (PID) algorithm implemented in a LabVIEW program on a personal computer (Fig. S6). The resistance of the temperature of the sensor was measured by a digital multimeter and the Peltier heater was connected to a DC power supply. By using the on-chip temperature and Peltier module, wide-range temperature control either above or below room temperature can be achieved in an accurate, rapid and integrated manner.

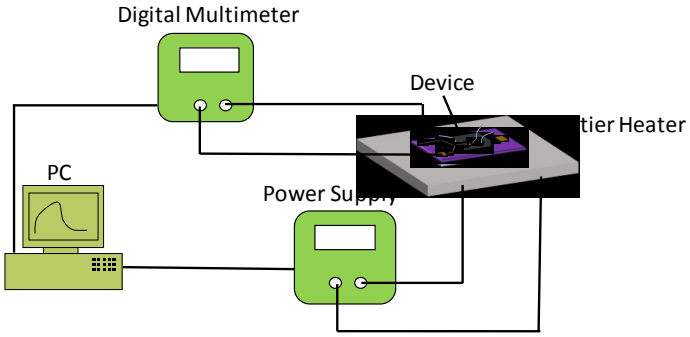

Fig. S6 Experimental setup for closed-loop temperature control.

Temperature sensor characterization: The temperature sensor was first calibrated at a series of temperatures. The measured resistance (R) of the thin film gold temperature sensor was observed to vary linearly with temperature (T). The dependence could be represented by the relationship $R=R_0[1+\alpha(T-T_0)]$, where R_0 is the sensor resistance at a reference temperature T_0, and α is the temperature coefficient of resistance (TCR) of the sensor. Fitting this relationship to the measurement data allowed determination of the parameter values, which were used to determine the chamber temperature from the measured sensor resistance during cell capture and release experiments. The temperature sensor typically had a measured resistance of 430.22 Ω at a reference temperature of 4 °C with a TCR of 3.01×10^{-3} 1/°C, as shown in Fig. S7.

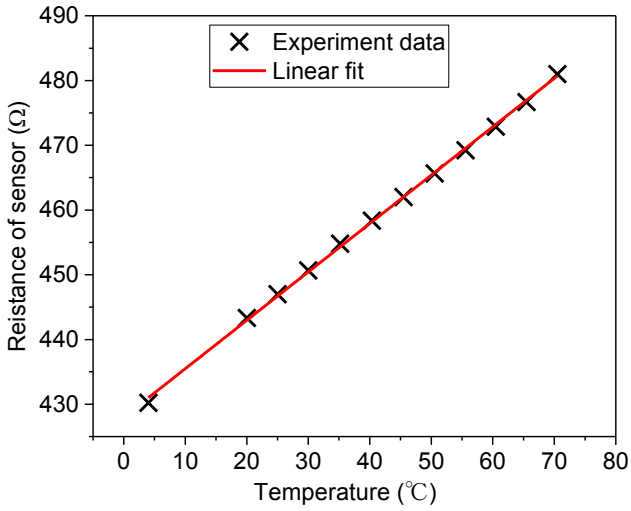

Fig. S7 Characterization of embedded temperature sensor. Resistance of temperature sensor (R) showing highly linear dependence on temperature (T). The solid line represents a linear fit to the experimental data with a regression equation: $R = 430.22[1+3.01\times10^{-3}(T-4)]$ (coefficient of determination R^2=0.999).

Simulation of temperature distribution: To evaluate the uniformity of the temperature distribution in the chamber, we performed numerical simulations using a three-dimensional steady-state heat transfer model.[2] The model considered the heat conduction in the chamber encapsulated by the silicon substrate (thermal conductivity: 149 W/m·K) and PDMS (thermal conductivity: 0.16 W/m·K) microfluidic channel with flow rate of buffer (thermal conductivity: 0.62 W/m·K) at 5 µL/min. The model is solved using the COMSOL Multiphysics software package. The cross-sectional profile of temperature distribution in the device at a flow rate 5 µL/min at 283.15 K (controlled by close-loop temperature control system) shown in Fig. S8a. It can be seen that the temperature in the chamber (~20 µm in height) was uniform. The extracted temperature distribution profile in the chamber shown in Fig. S8b demonstrated

a very small difference between the temperatures on the lower chamber surface and on the substrate surface where the recognition between IgE and D17.4 aptamer occurred. Based on this numerical analysis, it can be concluded that the temperature distribution was sufficiently uniform in the microfluidic chamber for the binding characterization.

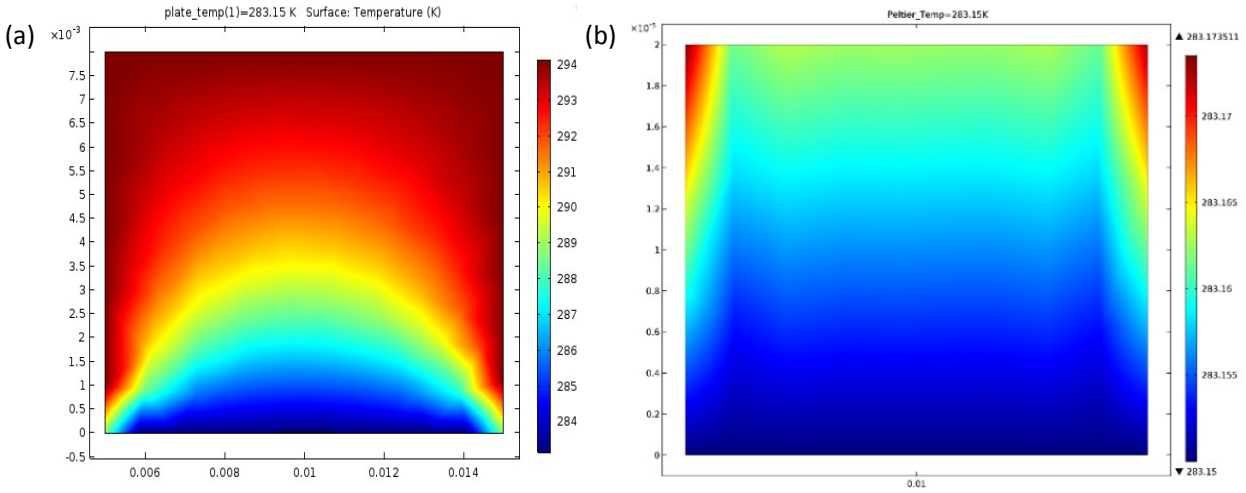

Fig. S8 Numerically-determined temperature distribution. Cross-sectional profile of (a) cross-section of device and (b) microfluidic channel. The results showed uniform temperature distribution in the microfluidic chamber.

References

(1) Zheng, C.; Huang, L.; Zhang, H.; Sun, Z.; Zhang, Z.; Zhang, G.-J., Fabrication of Ultrasensitive Field-Effect Transistor DNA Biosensors by a Directional Transfer Technique Based on CVD-Grown Graphene. *ACS Appl. Mater. Interfaces* **2015,** *7* (31), 16953-16959.

(2) Lin, Q.; Jiang, F.; Wang, X.-Q.; Xu, Y.; Han, Z.; Tai, Y.-C.; Lew, J.; Ho, C.-M., Experiments and simulations of MEMS thermal sensors for wall shear-stress measurements in aerodynamic control applications. *J. Micromech. Microeng* **2004,** *14* (12), 1640.